Dynamic Homogeneity by Architectural Design – Bottlebrush Polymers

Christos Grigoriadis, Alper Nese, Krzysztof Matyjaszewski, Tadeusz Pakula, Hans-Jürgen Butt, George Floudas*

The self-organization and dynamics of bottlebrush polymers consisting of poly(2-bromoisobutyryloxyethyl methacrylate) (PBiBEM) backbone and grafted n-butyl acrylate (PBA) chains are studied as a function of the side-chain length by X-ray scattering, dielectric spectroscopy, and rheology in relation to the respective homopolymers. All short-range correlations are dominated by the PBA side chains, whereas long-range correlations reflect the screening of the backbones by the side chains. Such correlations show up also in the segmental dynamics. The PBA segmental dynamics are slowed-down, whereas the backbone dynamics are plasticized by the side chains. Overall the bottle-brush architecture imparts dynamic homogeneity to the backbone and side-chain dynamics.

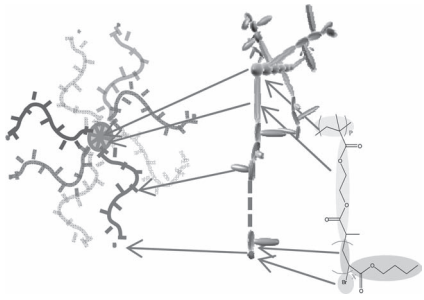

1. Introduction

Brush-like polymers consist of highly branched macromolecules where linear side chains are grafted to a backbone polymer chain. Due to their appearance, these molecules are known as cylindrical brush polymers or molecular bottlebrushes.[1–4] Their global conformation and physical properties are controlled by steric repulsion of the grafted side chains. Both conformation and properties can be controlled, at the synthesis level, by adjusting the grafting density and length of side chains. Molecules can switch their inherent conformation depending on external parameters such as temperature, solvent quality, pH, and ionic strength. Moreover their inherent elasticity makes them attractive for creating systems sensitive to external stimuli (as sensors, actuators). Lastly, synthetic brush-like polymers have their biological analogs, known as proteoglycans, that is, polyelectrolyte macromolecules consisting of a protein backbone and carbohydrate side chains.[2] The latter are responsible for various functions including mucociliary clearance of lung airways and mechanical performance of articular cartilage. It is thought that their brush-like structure with densely packed side chains is largely responsible for their functionality. Nowadays, molecular brushes can be synthesized by grafting-onto, grafting-through, and grafting-from methods. Most of the molecular brushes have been prepared by atom transfer radical polymerization (ATRP) using the latter method.[5–7]

The availability of bottlebrush polymers initiated several experimental and theoretical studies on their global conformation.[8–15] This issue, however, has been a point of debate. The reason for this complication is the presence of several length scales that include the contour length, the persistence length, and the cross-sectional radius. In any case, the equilibrium conformation results from the interplay between the repulsive forces due to the steric

C. Grigoriadis, Prof. G. Floudas
Department of Physics, University of Ioannina, P.O. Box 1186, GR-45110 Ioannina, Greece and Foundation for Research and Technology-Hellas (FORTH), Biomedical Research Institute (BRI), Ioannina, Greece;
E-mail: gfloudas@cc.uoi.gr
Dr. A. Nese, Prof. K. Matyjaszewski
Department of Chemistry, Center for Macromolecular Engineering, Carnegie Mellon University, 4400 Fifth Avenue, Pittsburgh, PA 15213, USA
Prof. T. Pakula, Prof. H.-J. Butt
Max-Planck-Institut für Polymerforschung, 55021 Mainz, Germany

DOI: 10.1002/macp.201200064

crowding of the side chains and the entropic restoring force of the backbone polymer. Recent Monte Carlo simulations under good solvent conditions revealed that the classical definition of a persistence length is not valid and that an effective persistence length can be defined instead by the cross-sectional diameter of the bottlebrush polymer.[14,15]

Apart from the conformational properties much less is known about the dynamics that are also affected by the global and local organization. Mostly the thermomechanical properties of linear and covalently crosslinked polymers have been investigated.[16–20] The viscoelastic properties of linear bottlebrush polymers comprising relatively short side chains attached to the polymer backbone were reminiscent to the behavior of the backbone polymer without side chains but containing an equivalent concentration of a small-molecule diluent.[16] In the case of the covalently crosslinked polymers, the emphasis was on the low equilibrium shear modulus (of the order of 1 kPa).[16,1] Again, this low modulus is more typical of a network swollen by a diluent (i.e. the term super-soft elastomers). However, here the diluent cannot be leached providing with additional potential biological applications.

The inherent dynamics of bottlebrush polymers have been much less investigated as they require separate probing of the backbone and side-chain dynamics. NMR and dielectric spectroscopy (DS)[21] are two techniques that have the required molecular specificity (proton chemical shift, dipole moment) that could probe the local molecular mobility in these intrinsically "heterogeneous" polymers. In a first such investigation[22] of brushes composed from a poly((2-(2-bromopropionyloxy)ethyl methacrylate-*stat*-methyl methacrylate (MMA)) backbone grafted with butyl acrylate (PBA) chains, by ^{1}H NMR, significant differences were reported in the spin-spin relaxation times belonging to the backbone and side-chains. The T_2 relaxation times for protons of MMA units in the backbone were significantly reduced with increasing side chain length and PBA grafting density. However, decoupling the molecular mobility from difference in the chemical environment is not an easy task by ^{1}H NMR.

In the present study, we investigate the backbone and side chain mobilities in bottlebrush polymers by dielectric spectroscopy. We employ two systems based on poly(2-bromoisobutyryloxyethyl methacrylate) (PBiBEM) backbone and PBA side chains with different degrees of polymerization. Before we proceed with the dynamics of the molecular brushes, we first investigate the homopolymer dynamics. As expected by the disparity in the glass temperatures of the respective homopolymers, the PBA and PBiBEM segmental dynamics vary by more than eight orders of magnitude when compared at the same temperature. However, in the brushes, there is a plasticization of the backbone dynamics and a somewhat slower side-chain dynamics, that is, dynamic homogeneity induced by architecture.

2. Experimental Section

2.1. Materials

2.1.1. Abbreviations

BA, n-butyl acrylate; EBiB, ethyl 2-bromoisobutyrate; dNbpy, 4,4′-di(5-nonyl)-2,2′-bipyridine; PMDETA, *N,N,N′,N″,N″*-pentamethyldiethylenetriamine; PBiBEM, poly(2-bromoisobutyryloxyethyl methacrylate). The molecular structures of the two homopolymers are depicted in Scheme 1.

2.1.2. Synthesis of PBA_{115}

A 10 mL Schlenk flask was charged with BA (6.68 g, 49.1 mmol), EBiB (60 μL, 0.409 mmol), PMDETA (43 μL, 4.91 mmol), and anisole (1.7 mL). The reaction mixture was degassed by two freeze-pump-thaw cycles. During the final cycle, the flask was filled with nitrogen and CuBr (0.0293 g, 0.205 mmol) was quickly added to the frozen mixture. The flask was sealed, evacuated, and back-filled with nitrogen three times before it was immersed in an oil bath at 60 °C. The polymerization was stopped after 5 h by cooling the flask to room temperature and exposing the reaction mixture to air. THF was added to the reaction mixture and the resulting polymer solution was purified by passing through a neutral alumina column. Polymer was dried by evaporating solvent and monomer under vacuum. $\overline{M}_{n,\,GPC}$ = 14 800 (calculated DP ≈ 115 by using PS standards), $\overline{M}_w/\overline{M}_n$ = 1.13.

2.1.3. Synthesis of PBA_{30}

A 10 mL Schlenk flask was charged with BA (6.00 g, 46.9 mmol), EBiB (229 μL, 1.56 mmol), PMDETA (65 μL, 1.56 mmol), and anisole (1.2 mL). The reaction mixture was degassed by two

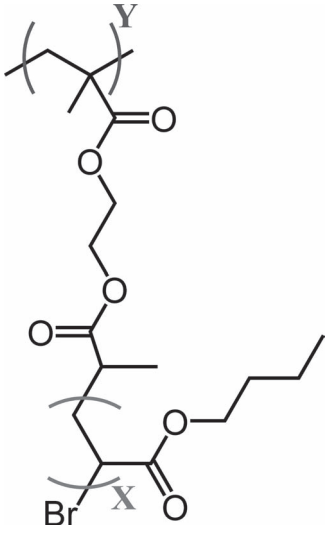

Scheme 1. Schematic of the molecular structure of the bottlebrushes investigated.

freeze-pump-thaw cycles. During the final cycle, the flask was filled with nitrogen and CuBr (0.0423 g, 0.296 mmol) was quickly added to the frozen mixture. The flask was sealed, evacuated, and back-filled with nitrogen three times before it was immersed in an oil bath at 70 °C. The polymerization was stopped after 2 h by cooling the flask to room temperature and exposing the reaction mixture to air. THF was added to the reaction mixture and the resulting polymer solution was purified by passing through a neutral alumina column and solvent and monomer were evaporated under vacuum. $\overline{M}_{n,\,GPC}$ = 4300 (calculated DP ≈ 30 by using PS standards), $\overline{M}_w/\overline{M}_n$ = 1.21.

2.1.4. Synthesis of PBA_{10}

A 10 mL Schlenk flask was charged with BA (6.68 g, 49.1 mmol), EBiB (229 μL, 1.56 mmol), PMDETA (0.722 mL, 4.91 mmol), and anisole (0.67 mL). The reaction mixture was degassed by two freeze-pump-thaw cycles. During the final cycle, the flask was filled with nitrogen and CuBr (0.0702 g, 0.491 mmol) was quickly added to the frozen mixture. The flask was sealed, evacuated, and back-filled with nitrogen three times before it was immersed in an oil bath at 60 °C. The polymerization was stopped after 4 h by cooling the flask to room temperature and exposing the reaction mixture to air. THF was added to the reaction mixture and the resulting polymer solution was purified by passing through a neutral alumina column. Monomer and solvent were evaporated under vacuum to obtain dry polymer. $\overline{M}_{n,GPC}$ = 1400 (calculated DP ≈ 10 by using PS standards), $\overline{M}_w/\overline{M}_n$ = 1.14.

2.1.5. Synthesis of $PBiBEM_{415}$-*g*-PBA_{10} and $PBiBEM_{415}$-*g*-PBA_{30}

$PBiBEM_{415}$ (0.147 g, 0.526 mmol, prepared by following a previous procedure),[23] BA (26.9 g, 210 mmol), 4,4′-di(5-nonyl)-2,2′-bipyridine (dNbpy), (0.215 g, 0.526 mmol), $CuBr_2$ (0.0029 g, 0.0132 mmol), and anisole (1.6 mL) were added to a 50 mL Schlenk flask and the reaction mixture was degassed by two freeze-pump-thaw cycles. At the last cycle CuBr (0.0358 g, 0.250 mmol) was added under nitrogen. The flask was placed in a preheated oil bath at 70 °C. Half of the reaction solution was taken out by syringe after 9 h. The polymerization was stopped after 22 h by cooling the flask to room temperature and opening the flask to air. The resulting polymer solutions were purified by precipitating three times from THF into cold methanol. The resulting polymers were dried under vacuum at room temperature for 24 h. Sample taken after 9 h should have an average DP_{sc} of BA = 10 as determined by gravimetry and assuming quantitative initiation. However, this value should be DP_{sc} = 25 since at 2.5% monomer conversion initiation efficiency should be ≈40% under the selected reaction conditions,[24] $\overline{M}_{n,\,GPC}$ = 197 000, $\overline{M}_w/\overline{M}_n$ = 1.12. Final polymer sample after 22 h should have an average DP_{sc} of BA = 30. However, this value should be DP_{sc} = 37.5 since at 7.5% monomer conversion initiation efficiency should be ≈80%,[24] $\overline{M}_{n,\,GPC}$ = 302 000, $\overline{M}_w/\overline{M}_n$ = 1.25. In the description of the samples analyzed in this paper, we use values of DP_{sc} calculated for the quantitative initiation.

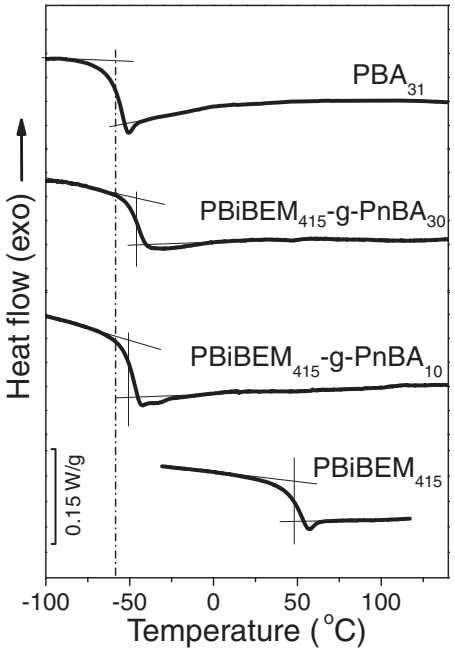

Figure 1. DSC thermograms of the homopolymers and bottlebrushes. The vertical line is the glass temperature of PBA_{30}.

2.2. Differential Scanning Calorimetry

The thermal behavior was determined by differential scanning calorimetry (DSC) on cooling and subsequent heating at a rate of 10 K min^{-1} with a Mettler 30 DSC under N_2 atmosphere. The DSC traces from the second heating scan of two homopolymers and the corresponding bottlebrushes are shown in Figure 1.

2.3. X-Ray Scattering

Both wide-angle and small-angle X-ray scattering (WAXS/SAXS) measurements have been performed from powder or liquid samples using a pinhole collimator and a two-dimensional detector (Bruker) with 1024Í1024 pixels. A graphite monochromator was used (λ = 0.154 nm), and the sample-to-detector distance was 7.3 cm. Measurements of 1 h long were made within the temperature range from 303 to 423 on heating and on subsequent cooling in steps of 10 K. The recorded 2-D scattered intensities were investigated over the azimuthal angle and are presented as a function of the scattering wave vector q ($q = (4\pi/\lambda)\sin(2\theta/2)$, where 2θ is the scattering angle). In the SAXS measurements, the sample-to-detector distance was set at 1.78 m. 2-D images were obtained for different temperatures in the range $303 < T < 453$ K in 10 K intervals on heating and subsequent cooling. Longer SAXS measurements (12 to 16 h) were made for two **$PBiBEM_{400}$-*g*-PBA_{50}** brushes with and without Br substitution at 298 K.

2.4. Rheology

An advanced rheometric expansion system equipped with a force-rebalanced transducer was used in the oscillatory mode

for recording the viscoelastic properties of the bottlebrushes. Depending on the temperature range, two transducers were used with 2000, 2 g cm and 200, 0.2 g cm upper and lower sensitivity, respectively. The sample was prepared on the lower plate of the 10 mm diameter parallel plate geometry setup and heated under a nitrogen atmosphere until it could flow. Subsequently, the upper plate was brought into contact, the gap thickness was adjusted to 1 mm, and the sample was slowly cooled to the desired starting temperature. The storage (G') and loss (G'') shear moduli of the two bottlebrushes **PBiBEM**$_{415}$-*g*-**PBA**$_{10}$ and **PBiBEM**$_{415}$-*g*-**PBA**$_{30}$ were monitored in different types of experiments. First, the linear and nonlinear viscoelastic ranges were identified, by recording the strain amplitude dependence of the complex shear modulus $|G^*|$at selected temperatures. In the subsequent experiments strain amplitudes within the linear viscoelastic range were used. These experiments involved isothermal frequency scans within the range $10^{-1} < \omega < 10^{2}$ rad s^{-1} for different temperatures in the range from 226 to 363 K. Master-curves of the shear moduli were obtained according to

$$G*(\omega;T) = b_T G*(a_T\omega;T_{ref}) \quad (1)$$

where b_T and a_T are single modulus-scale (vertical) and single frequency-scale (horizontal) shift factors that allow superposition of all viscoelastic data at each temperature T with the results at the reference temperature (T_{ref} = 233 K). At the reference temperature the strain amplitude was typically 0.02% for both bottlebrushes.

2.5. Dielectric Spectroscopy (DS)

Dielectric measurements were made under "isobaric" conditions as a function of temperature and under "isothermal" conditions as a function of pressure. The "isobaric" measurements were performed at different temperatures in the range 123.15–423.15 K, at atmospheric pressure, and for frequencies in the range from 10^{-2} to 10^{6} Hz. The "isothermal" measurements were made for the **PBA**$_{30}$ homopolymer for temperatures in the range from 255 to 295 K and for pressure up to 300 MPa. The measurements under hydrostatic pressure were carried out in a Novocontrol pressure cell. The pressure setup consists of a temperature controlled cell, hydraulic closing press with air pump, and air pump for hydrostatic test pressure.[25] The sample cell is isolated with a Teflon ring from the surrounding silicone oil that is the pressure transmitting liquid. The "isothermal" frequency sweeps were made with a temperature stability better than ±0.1 K, and a pressure stability better than ±2 MPa. In every case, the complex dielectric permittivity $\varepsilon^* = \varepsilon' - i\varepsilon''$, where ε' is the real and ε'' is the imaginary part, was obtained as a function of frequency ω, temperature T, and pressure P, that is, $\varepsilon^*(T,P,\omega)$.[25,26] The analysis of both T- and P-dependent experiments was made using the empirical equation of Havriliak and Negami (HN):

$$\varepsilon*(T,P,\omega) = \varepsilon_\infty(T,P) + \frac{\Delta\varepsilon(T,P)}{\left[1+(i\omega\tau_{HN}(T,P))^m\right]^n} + \frac{\sigma_0(T,P)}{i\varepsilon_f\omega} \quad (2)$$

where $\varepsilon_\infty(T,P)$ is the high-frequency permittivity, $\tau_{HN}(T,P)$ is the characteristic relaxation time in this equation, $\Delta\varepsilon(T,P) = \varepsilon_0(T,P) - \varepsilon_\infty(T,P)$ is the relaxation strength, m, n (with limits $0 < m$, $mn \leq 1$) describe, respectively, the symmetrical and asymmetrical broadening of the distribution of relaxation times, σ_o is the dc-conductivity and ε_f is the permittivity of free space. From τ_{HN}, the relaxation time at maximum loss, τ_{max}, is obtained analytically following

$$\tau_{max} = \tau_{HN}\left[\frac{\sin\left(\frac{\pi m}{2+2n}\right)}{\sin\left(\frac{\pi mn}{2+2n}\right)}\right]^{-1/m} \quad (3)$$

At lower frequencies, ε'' rises due to the conductivity ($\varepsilon'' = \sigma/(\omega\varepsilon_f)$). The measured ε'' spectra have been used for the analysis except at high temperatures where the derivative of ε' has been employed ($d\varepsilon'/d\ln\omega \approx -(2/\pi)\varepsilon''$). This method is useful in fitting relaxation processes which are hidden under the conductivity, provided that the system is free of surface polarization effects.

3. Results and Discussion

3.1. Homopolymer Dynamics

The DSC traces of the bottlebrushes revealed a single glass temperature in the proximity of the PBA T_g. However, based on this information alone no definite conclusions can be made with respect to the backbone mobility in the bottlebrushes. Instead, detailed information on the homopolymer and bottlebrush dynamics can be obtained by following the dipolar response to an external electric field through DS. We first report on the homopolymer dynamics. Figure 2 provides with the relaxation times at maximum dielectric loss, τ_{max}, for the PBiBEM$_{415}$ homopolymer at temperatures both below and above the glass temperature. Figure S1 (Supporting Information) shows shifted curves (i.e. master curves) of all three quantities (σ^*, ε^*, M^*) in the

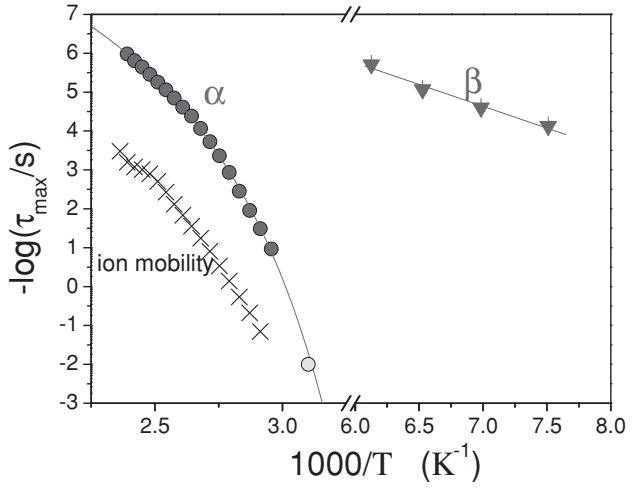

Figure 2. Arrhenius relaxation map of the **PBiBEM**$_{415}$ relaxation times; (filled circles): segmental (α-) relaxation times, (filled triangles): β-process, (X): ion mobility. The yellow circle is the DSC T_g (τ = 100s).

same representation. The Figure displays "master curves" of the conductivity σ^* (= $\sigma' + i\sigma''$), the dielectric function ε^* (= $\varepsilon' - i\varepsilon''$) and the electric modulus M^* (= $M' + iM''$) of PBiBEM at the same reference temperature. The superpositions were made around the M'' maximum related to the ionic relaxation and the same horizontal shift factors (a_T) were applied in the ε^* and σ^* representations. In all representations, the crossing of the real and imaginary parts occurs at the same frequency signifying the rate of the process due to the ionic mobility (dashed line). At frequencies below the frequency of ion mobility, the M' and M'' data display slopes of 2 and 1, respectively. At much lower frequencies, the increase of the ε' and ε'' is due to the electrode polarization (EP) process. As expected, the EP process shows up also in the other representations but with a different weight. At frequencies higher than the characteristic frequencies of ion motion, the ε^* and M^* spectra are dominated by the dipolar motions (α-process in the shown T-range) that are of interest here.

The relaxation times for the α-process of $PBiBEM_{415}$ (Figure 2) conform to the Vogel–Fulcher–Tammann (VFT) equation:

$$\tau = \tau_0 \exp\left(\frac{D_T T_0}{T - T_0}\right) \quad (4)$$

where τ_0 (= 1.4×10^{-11} s) is the relaxation time in the limit of very high temperatures, D_T (= 6.70 ± 0.59) is the activation parameter and T_0 (= 262 ± 3 K) is the "ideal" glass temperature. The glass temperature for $PBiBEM_{415}$ is at 321 K (defined at $\tau \approx 100$ s) and is in good agreement with the DSC T_g. The α-process here reflects the dynamics of the polar side ester groups that are influenced both by the backbone and side group mobility. In the same figure, a local (β-process) is included with an Arrhenius T-dependence ($\tau = \tau^* \exp(E/k_B T)$) with a limiting relaxation time at high temperatures of $\tau^* = 3 \times 10^{-13}$ s and activation energy of 21 kJ mol^{-1}, reflecting a local relaxation of the side ester groups in a frozen backbone.

Figure 3 provides the corresponding relaxation times for PBA_{30} (the superimposed spectra are shown in Figure S2, Supporting Information). Apart from the local process with an Arrhenius T-dependence ($\tau^* = 5 \times 10^{-15}$ s, activation energy ≈27 kJ mol^{-1}) the main finding is of two processes at and above the glass temperature, indicated as α and α', displaying a different T-dependence. The processes are characterized by the parameters $\tau_0 = 1.7 \times 10^{-11}$ s, $D_T = 4.64 \pm 0.22$, $T_0 = 189 \pm 1$ K, and $T_g = 218.8$ K for α. For the slower α'-process, we obtained $\tau_0 = 2 \times 10^{-10}$ s, D_T = 5.89 ± 0.22, T_0 = 179 ± 1 K, and T_g = 218.8 K. The latter is responsible for the breakdown of time–temperature superposition (tTs) seen in Figure S2 (Supporting Information). The two processes merge when decreasing temperature giving rise to a single glass temperature that is in agreement with the single DSC T_g.

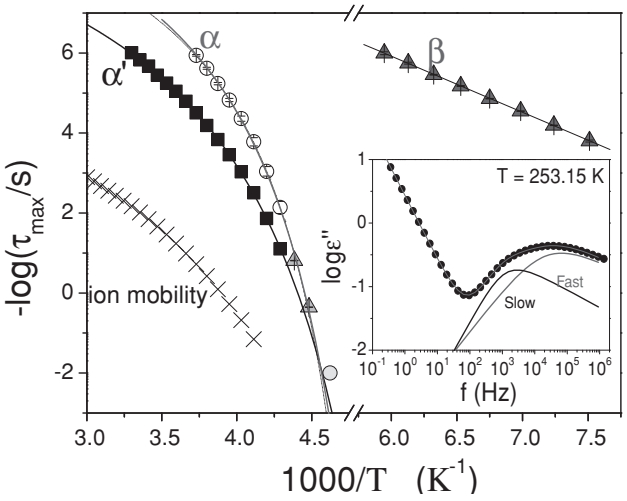

Figure 3. Arrhenius relaxation map of the **PBA_{30}** relaxation times corresponding to the α (open circles), α' (filled squares), β (triangles) and (X) ion mobility processes. In the inset a representative fit to the dielectric loss curve at 253.15 K is shown, where the "fast" and "slow" processes correspond to the α and α' processes, respectively. The yellow circle is the DSC T_g (τ = 100s).

To explore the origin of the dual segmental process we have studied the molecular weight dependence by employing three PBA_x homopolymers with x = 10, 30, and 115. The result for the segmental processes is shown in Figure 4 in a T_g-scaled representation. Both processes are independent of the molecular weight revealing, which indicates their local segmental character rather than being caused by an overall translation of the chain (Rouse like).

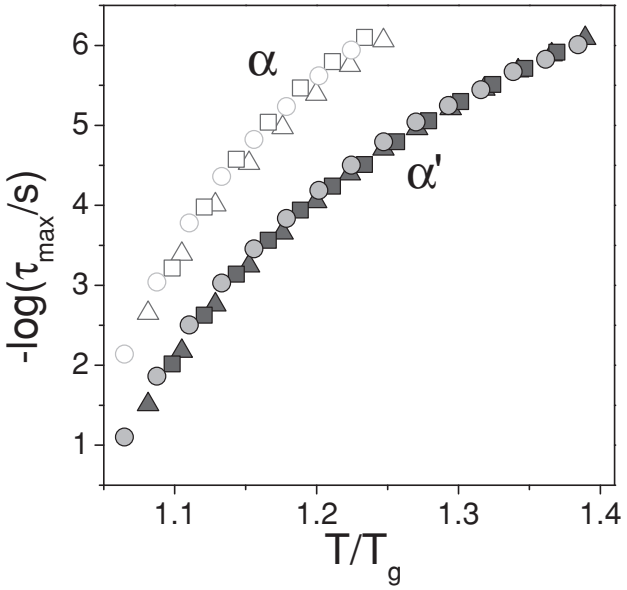

Figure 4. T_g-normalized relaxation times of the α (open symbols) and α' (filled symbols) relaxation processes in three PBA homopolymers with degrees of polymerization: (triangles) x = 10, (circles): x = 30 and (squares): x = 115.

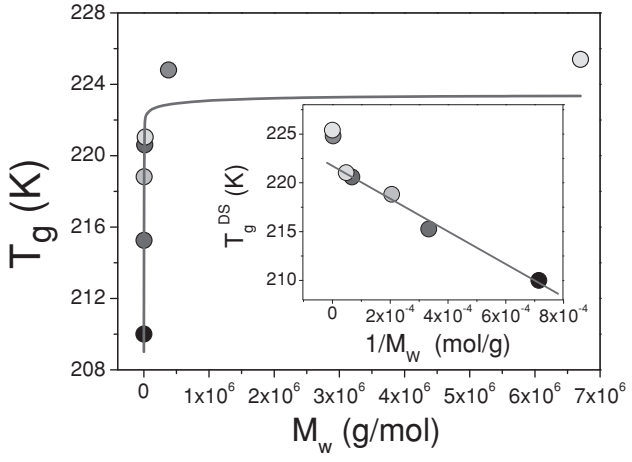

Figure 5. Molecular mass dependence of the glass temperature in PBA including literature data[26–28] in addition to data from the present investigation. Inset: the same data are plotted versus the inverse molecular mass and the line is the result of the fit to the Fox–Flory equation for the lower molecular mass samples.

The dependence of the glass temperature on the PBA molecular weight is shown in Figure 5. The figure includes additional literature data on the segmental dynamics of PBA.[27–29] The dependence follows only approximately the Fox–Flory equation, known to be valid only within a limited range of molecular weights.

$$T_g = 221.7 \pm 0.4 - \frac{16800 \pm 1100}{M_w} \quad (5)$$

The fact that we observed two segmental modes could be, in principle, caused by an impurity such as remaining copper catalyst. Residual copper/ligand complexes may result in crosslinking reactions by reacting with the —Br chain end.[23] However, a dual segmental process was also observed in the bottlebrushes (see below) that were precipitated into methanol that removes the catalyst almost completely. Alternatively, the dual segmental process can result from the proposed nanophase separation in side-chain polymers bearing long akyl groups.[30,31] These alkyl nanodomains are characterized by a polyethylene-like glass temperature that is lower than the backbone T_g. The two modes shown in Figure 4 agree with the proposed nanophase separation in poly(alkyl acrylates).The role of pressure as a separator of molecular processes is well known and relies in the different pressure sensitivity of different modes.[25,26,32] In an effort to obtain further insight on the dual segmental processes of PBA, we employ pressure as an additional thermodynamic parameter in order to separate the two modes further (Figure 6). The relaxation times of both processes slow-down with pressure and conform to the modified VFT equation for pressure dependent studies:[33]

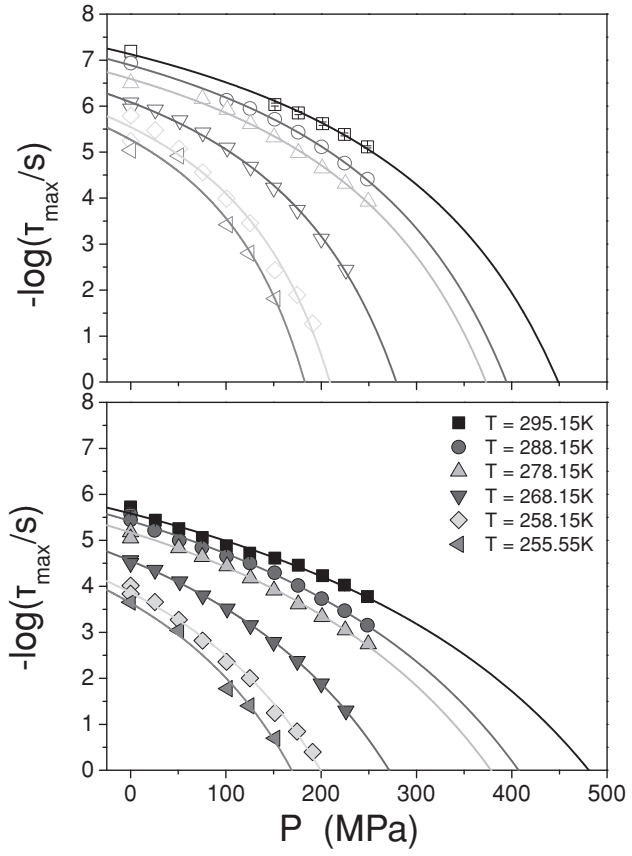

Figure 6. Pressure dependence of the relaxation times corresponding to the fast (α) (top) and slower (α') (bottom) processes of $\mathbf{PBA}_{30}$ at different temperatures as indicated.

$$\tau = \tau_0^* \exp\left(\frac{D_P p}{p_0 - p}\right) \quad (6)$$

We obtained $D_P = 8$ and 10.7 for the "fast" and "slow" processes, respectively. From each "isotherm" a characteristic pressure (P_g) could be extracted when the relaxation time is at 100 s and the resulting $T(P)$ dependence is plotted in Figure 7 for the α and α' processes. Both dependencies agree with[34]

$$T_g(P) = T_g(0)\left(1 + \frac{\kappa}{\lambda}P\right)^{1/\kappa} \quad (7)$$

with corresponding parameters $T_g(0)$, κ, λ and $dT_g/dP|_{P\to 0}$ of 223.7 K, 1.60, 1402 MPa and 0.16 K/MPa for the faster α process and 224.9 K, 3.20, 1216 MPa and 0.18 K/MPa for the slower α' process. Thus, the two modes possess only slightly different pressure sensitivity. This observation provides further evidence that they reflect intrinsic polymer segmental dynamics.

3.2. Structure of Bottlebrushes

The global and local organization in the bottlebrushes can be studied by X-ray scattering at small and wide angles,

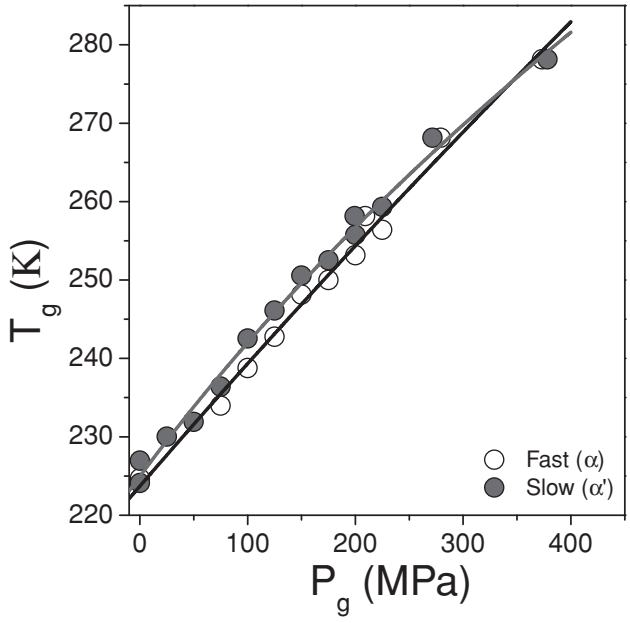

Figure 7. Pressure dependence of the glass temperatures corresponding to the "fast" (α) (open circles) and "slow" (α') (filled circles) processes of PBA_{31}.

respectively. Figure 8 provides the WAXS curves of the homopolymers and respective bottlebrushes at 298 K. The 2D scattering patterns are also shown. The PBA scattering curve contains two maxima. The corresponding distances were calculated from $d = 2\pi z/q$, where $z = 1.23$ accounts for nearest neighbor correlations only.[35,18] The corresponding distances at 0.57 and 1.49 nm reflect van der Waals nearest neighbor correlations and longer-range intermolecular correlations, respectively. In PBiBEM, a single maximum is obtained corresponding to an intermediate distance of 0.67 nm. In the molecular brushes, all short-range correlations (WAXS) are dominated by the PBA brushes. On the contrary, all long-range correlations (SAXS) are dominated by the contrast between the PBiBEM backbone and the PBA brushes as shown by the SAXS curves plotted as a function of the PBA degree of polymerization. The figure indicates an increasing separation and screening of the PBiBEM backbones with increasing PBA degree of polymerization.

More informative representation of the scaling of the backbone–backbone correlation distances is by making a double logarithmic plot of the distances as a function of the molar mass of the macromonomer M. This representation is shown in Figure 9. The Figure contains the results from a $PBiBEM_{415}$-g-PBA_{50} without the end–Br group synthesized for the present investigation. A line with a slope of ≈0.3 could suggest an extension of the cylinder length formed by the bottlebrush with increasing the molar mass of the side chain. The length of extension of the brush molecules per monomer unit of the backbone, l_m, can be estimated from the cylinder length per monomer as $l_m = 4M/\pi\rho N_A d^2$, where ρ is the density of PBA (1.09 g cm^{-3}), N_A is Avogadro's number and d is the intermolecular distance obtained from SAXS. The result for l_m is shown also in Figure 9 as a function of the molar mass of the macromonomer. It shows an increasing cylinder length per

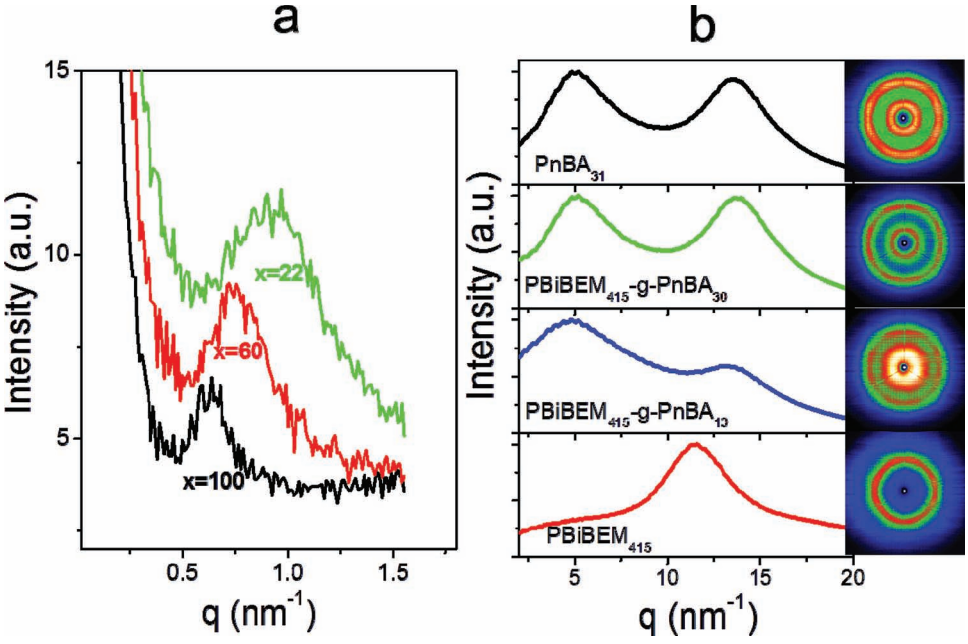

Figure 8. (a) SAXS curves of the **$PBiBEM_{415}$-g-PBA_x** brushes at 298 K. (b) WAXS curves of the homopolymers and respective brushes at 298 K. The corresponding 2D images are also shown. Notice that all short distance correlations in the bottlebrushes are dominated by the PBA side chains.

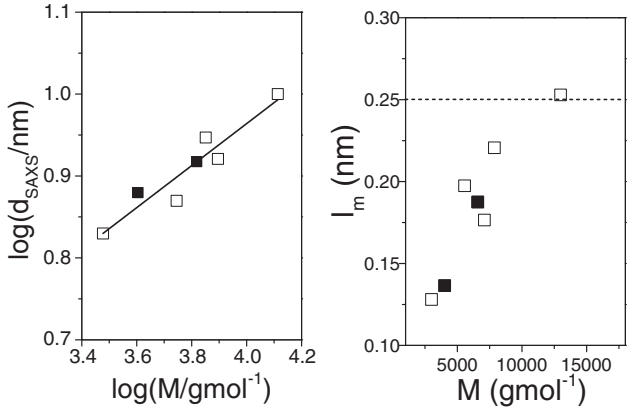

Figure 9. (Left): SAXS inter-molecular distance plotted as a function of the molar mass of the macromonomer, *M* in a double logarithmic plot. The open symbols are from systems measured earlier by T. Pakula and the filled symbols are from the present investigation. (Right): Length of the brush molecules per monomer unit of the backbone, l_m, plotted as a function of the molar mass of the macromonomer. The dashed line indicates the maximum length corresponding to the all-*trans* conformation of an aliphatic chain.

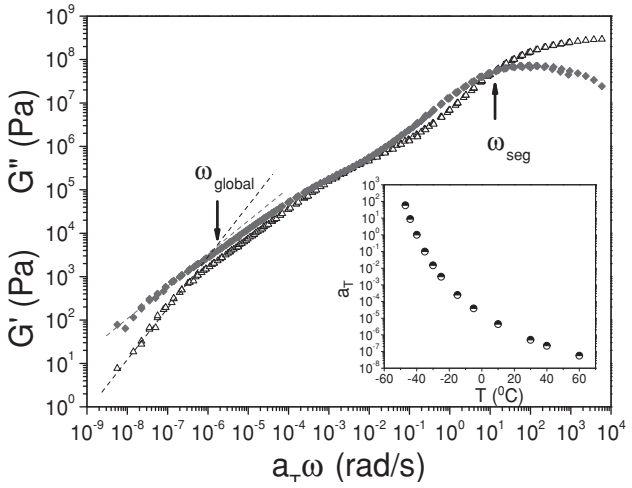

Figure 10. Reduced frequency plots for the storage (open symbols) and loss (filled symbols) moduli of the **PBiBEM$_{415}$-*g*-PBA$_{30}$** bottlebrush at a reference temperature of 233 K. The characteristic frequencies corresponding to the segmental and global polymer processes at the reference temperature are indicated by arrows as well as the temperature dependence of the shift factors a_T (inset).

backbone monomer with increasing length of the side chain. Notice that values of 0.14 and 0.19 are obtained here for the PBiBEM$_{415}$-*g*-PBA$_{30}$ and PBiBEM$_{415}$-*g*-PBA$_{50}$ bottlebrushes that are below the limiting value of 0.25 nm corresponding to the all-*trans* conformation of an aliphatic chain. Therefore, the investigated bottlebrushes, bearing relatively short chains, retain some conformational freedom at the backbone level and this is expected to have consequences on the dynamics.

3.3. Dynamics of Molecular Brushes

The dynamics of the bottlebrushes was studied both by rheology and DS. Rheology, can in principle, provide the full-spectrum of relaxations; starting from the relaxation of the segments, to the relaxation of the arms and to the global relaxation. In rheology, master-curves of *G′* and *G″* at a reference temperature have been obtained using the time–temperature superposition. This procedure provided the temperature dependence of the shift factors a_T. Figure 10 gives the superimposed storage and loss moduli of **PBiBEM$_{415}$-*g*-PBA$_{30}$** bottlebrush at a reference temperature of 233 K. The relaxation times corresponding to the segmental process were obtained from $\tau(T_{ref}) = 2\pi/\omega_{seg}$, where ω_{seg} is the frequency corresponding to the crossing of *G′* and G″ at the reference temperature. It is not surprising that a single dynamic process is seen in rheology in view of the proximity of the two modes (α and α' in DS) and the smaller frequency range available. At low reduced frequencies (high temperatures), the moduli display terminal zone behavior with the expected frequency dependence: $G' \approx \omega^2$ and $G'' \approx \omega$. In the intermediate frequency range (at $\alpha_T\omega \approx 10^{-3}$), there is an indication for the PBA arm relaxation. Segmental and global polymer relaxation times at other temperatures than the reference were obtained from $\log\tau(\tau) = \log\tau(T_{ref}) + \log\alpha_T$. The characteristic times of the PBA segmental dynamics in the **PBiBEM$_{415}$-*g*-PBA$_{30}$** bottlebrush as obtained from rheology and DS are compared in Figure S3 (Supporting Information). The single segmental process from rheology bisects the dual segmental process obtained from DS.

In DS, the spectra revealed the presence of several dielectrically active processes (Figure S4, Supporting Information). At lower temperatures, the dual segmental process of PBA is evident, however, with longer relaxation times as compared to a PBA homopolymer of the same degree of polymerization. At low frequencies, the calculated dielectric loss data (from the derivative of ε' with respect to frequency) display a narrow process associated with the mobility of residual ions. At intermediate frequencies, the weak process reflects the modified PBiBEM dynamics in the molecular brush. The low dielectric strength of this process complies with the lower strength of PBiBEM segmental dynamics as compared to the PBA segmental dynamics ($T\Delta\varepsilon$(PBA)/$T\Delta\varepsilon$(PBiBEM)≈3). Figure 11 gives the relaxation times in the **PBiBEM$_{415}$-*g*-PBA$_{10}$** bottlebrush, obtained from DS, that correspond to the modified backbone (PBiBEM) and side-chain (PBA) local segmental dynamics. For comparison, the homopolymer dynamics is also shown by dashed (PBiBEM) and dash-dotted (PBA)

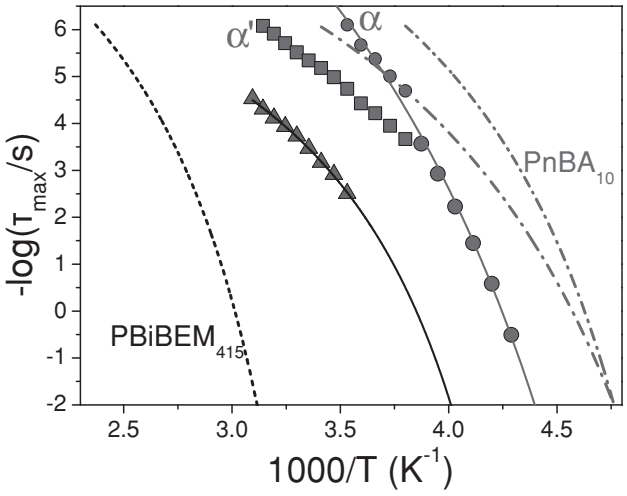

Figure 11. Arrhenius relaxation times of the different processes in the **PBiBEM$_{415}$-*g*-PBA$_{10}$** bottlebrush corresponding to the α (circles) and α' (squares) processes of PBA, and to the backbone (PBiBEM) segmental process (up triangles) in the copolymer. The PBA$_{10}$ and PBiBEM$_{415}$ homopolymer relaxation times are shown with a dash-dotted and dashed lines, respectively.

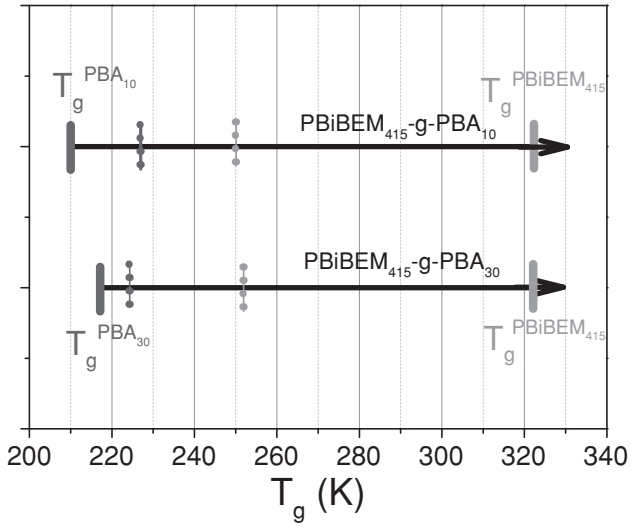

Figure 12. Glass temperatures in the two homopolymers (solid vertical lines) and the respective bottlebrushes (dashed lines). In blue (red) are the glass temperatures of the PBA (PBiBEM).

lines. The figure depicts modified segmental dynamics in the copolymer brushes as compared to the homopolymers. The side chain dynamics is slowed-down as compared to a homopolymer chain with the same degree of polymerization, possibly reflecting the restrictions imposed by the backbone and the strong intermolecular interactions of the perturbed side chains. On the other hand, the backbone dynamics (PBiBEM) is plasticized by the side chains (PBA). This effect is reminiscent to the internal plasticization found, for example, in poly(n-alkyl methacrylates).[31,36,37] The copolymers are still dynamically heterogeneous as they possess different time scales for the side chain and backbone dynamics that are 2–3 decades apart. Yet, these can be considered as dynamically homogeneous when compared to the corresponding homopolymers.

This situation on the induced dynamic homogeneity in the bottlebrushes is depicted schematically in Figure 12 where the glass temperatures (defined at $\tau = 100$ s) are compared to the respective homopolymer glass temperatures. According to Figure 12, the bottlebrush **PBiBEM$_{415}$-*g*-PBA$_{10}$** is dynamically more homogeneous (component T_g difference of ≈22 K) than as compared to **PBiBEM$_{415}$-*g*-PBA$_{30}$** (component T_g difference of ≈30 K) and this is despite the lower T_g of PBA$_{10}$. The reason for this is the higher restriction on the local segmental modes of PBA by the less mobile backbone. Nevertheless, the main conclusion is that homopolymer dynamics with a glass temperature disparity of ≈110 K and segmental relaxation times that differ by more than eight orders of magnitude become dynamically more homogeneous when combined in a bottlebrush polymer. This may suggest that other dense heterogeneous systems (synthetic or biological) could become dynamically more homogenous by the molecular design.

4. Conclusion

Local and global correlations in the molecular brushes were found to be dominated by correlations between the PBA side chains and PBiBEM backbones, respectively. The densely grafted side chains can stiffen the polymer backbone but it retains some conformational freedom. Dielectric spectroscopy allowed investigating the site-specific dynamics in the same bottlebrush polymers. It was shown that the side chain and backbone dynamics are altered compared to the respective homopolymers and the molecule becomes dynamically more homogeneous. The induced dynamic homogeneity by architectural design may have consequences on the physical properties of other molecular dense systems such as branched stars and networks. In addition, it would be of interest to explore the role of dynamic homogeneity in their corresponding biological analogs.

Supporting Information

Supporting Information is available from the Wiley Online Library or from the author.

Acknowledgements: The current work was supported by the Research unit on Dynamics and Thermodynamics of the

UoI co-financed by the European Union and the Greek state under NSRF 2007-2013 (Region of Epirus, call 18). In addition is co-funded by the European Union - European Social Fund (ESF) & National Sources, in the framework of the program "THALIS" of the "Operational Program Education and Life Long Learning" of the Hellenic Ministry of Education, Life Long Learning and religious affairs, and the National Science Foundation (DMR 09-69301).

Received: February 9, 2012; Revised: March 15, 2012; Published online: May 18, 2012; DOI: 10.1002/macp.201200064

Keywords: brush-like polymers; dielectric spectroscopy; dynamics; heterogeneity

[1] K. Matyjaszewski, N. V. Tsarevsky, *Nat. Chem.* **2009**, *1*, 276.
[2] S. S. Sheiko, B. S. Sumerlin, K. Matyjaszewski, *Prog. Polym. Sci.* **2008**, *33*, 759.
[3] H. G. Börner, K. Beers, K. Matyjaszewski, S. S. Sheiko, M. Möller, *Macromolecules* **2001**, *34*, 4375.
[4] K. L. Beers, S. G. Gaynor, K. Matyjaszewski, S. S. Sheiko, M. Moeller, *Macromolecules* **1998**, *31*, 9413.
[5] K. Matyjaszewski, N. V. Tsarevsky, *Nat. Chem.* **2009**, *1*, 276.
[6] K. Matyjaszewski, J. Xia, *Chem. Rev.* (Washington, D. C.) **2001**, *101*, 2921.
[7] N. V. Tsarevsky, K. Matyjaszewski, *Chem. Rev.* (Washington, DC, United States) **2007**, *107*, 2270.
[8] A. Gauger, T. Pakula, *Macromolecules* **1995**, *28*, 190.
[9] M. Saariaho, O. Ikkala, I. Szleifer, G. ten Brinke, *J. Chem. Phys.* **1997**, *107*, 3267.
[10] S. Elli, F. Ganazzoli, E. G. Timoshenko, Y. A. Kuznetsov, R. Connolly, *J. Chem. Phys.* **2004**, *120*, 6257.
[11] S. Rathgeber, T. Pakula, A. Wilk, K. Matyjaszewski, K. L. Beers, *J. Chem. Phys.* **2005**, *122*, 12490.
[12] B. Zhang, F. Gröhn, J. S. Pedersen, K. Fischer, M. Schmidt, *Macromolecules* **2006**, *39*, 8440.
[13] S. Bolisetty, C. Airaud, Y. Xu, A. H. E. Müller, L. Harnau, S. Rosenfeldt, P. Lindner, M. Ballauff, *Phys. Rev. E.* **2007**, *75*, 040803.
[14] H.-P. Hsu, W. Paul, K. Binder, *Macromolecules* **2010**, *43*, 3094.
[15] H.-P. Hsu, W. Paul, K. Binder, *Macromol. Theory Simul.* **2011**, *30*, 510.
[16] T. Pakula, Y. Zhang, K. Matyjaszewski, H.-I. Lee, H. Boerner, S. Qin, G. C. Berry, *Polymer* **2006**, *47*, 7198.
[17] L. Okrasa, T. Pakula, Y. Inoue, K. Matyjaszewski, *Colloid Polym. Sci.* **2004**, *282*, 844.
[18] B. Zhang, S. Zhang, L. Okrasa, T. Pakula, T. Stephan, M. Schmidt, *Polymer* **2004**, *45*, 4009.
[19] D. Neugebauer, Y. Zhang, T. Pakula, S. S. Sheiko, K. Matyjaszewski, *Macromolecules* **2003**, *36*, 6746.
[20] W. Jakubowski, A. Juhari, A. Best, K. Koynov, T. Pakula, K. Matyjaszewski, *Polymer* **2008**, *49*, 1567.
[21] A. Gitsas, G. Floudas, H.-J. Butt, T. Pakula, K. Matyjaszewski, *Macromolecules* **2010**, *43*, 2453.
[22] J. Pietrasik, B. S. Sumerlin, H.-I. Lee, R. R. Gil, K. Matyjaszewski, *Polymer* **2007**, *48*, 496.
[23] A. Nese, S. S. Sheiko, K. Matyjaszewski, *Eur. Polym. J.* **2011**, *47*, 1198.
[24] B. S. Sumerlin, D. Neugebauer, K. Matyjaszewski, *Macromolecules* **2005**, *38*, 702.
[25] G. Floudas, *Prog. Polym. Sci.* **2004**, *29*, 1143.
[26] G. Floudas, M. Paluch, A. Grzybowski, K. L. Ngai, *Molecular Dynamics of Glass-Forming Systems. Effects of Pressure*, Springer-Verlag, Berlin, **2011**.
[27] T. Hayakawa, K. Adachi, *Macromolecules* **2000**, *33*, 6834.
[28] D. Fioretto, A. Livi, P. A. Rolla, G. Socino, L. Verdini, *J. Phys. C* **1994**, *6*, 5295.
[29] J. L. Gomez Ribelles, J. M. Meseguer Duenas, M. M. Pradas, *J. Appl. Polym. Sci.* **1989**, *38*, 1145.
[30] M. Beiner, H. Huth, *Nat. Mater.* **2003**, *2*, 595.
[31] G. Floudas, P. Stepanek, *Macromolecules* **1998**, *31*, 6951.
[32] K. Mpoukouvalas, G. Floudas, G. Williams, *Macromolecules* **2009**, *42*, 4690.
[33] M. Plauch, A. Patkowski, E. W. Fischer, *Phys. Rev. Lett.* **2000**, *85*, 2140.
[34] S. P. Andersson, O. Andersson, *Macromolecules* **1998**, *31*, 2999.
[35] A. Guinier, *X-ray Diffraction in Crystals, Imperfect Crystals and Amoprhous Bodies*, W.H. Freeman, San Fransisco, **1963**.
[36] M. Mierzwa, G. Floudas, P. Stepanek, G. Wegner, *Phys. Rev. B.* **2000**, *62*, 14012.
[37] G. Floudas, P. Placke, P. Stepanek, W. Brown, G. Fytas, K. L. Ngai, *Macromolecules* **1995**, *28*, 6799.